Runaway tails in magnetized plasmas

E. Moghaddam-Taaheri, L. Vlahos, H. L. Rowland, and K. Papadopoulos
Department of Physics and Astronomy, University of Maryland, College Park, Maryland 20742

(Received 1 July 1985; accepted 5 August 1985)

The evolution of a runaway tail driven by a dc electric field in a magnetized plasma is analyzed. Depending on the strength of the electric field and the ratio of plasma to gyrofrequency, there are three different regimes in the evolution of the tail. The tail can be (a) stable with electrons accelerated to large parallel velocities, (b) unstable to Čerenkov resonance because of the depletion of the bulk and the formation of a positive slope, (c) unstable to the anomalous Doppler resonance instability driven by the large velocity anisotropy in the tail. Once an instability is triggered (Čerenkov or anomalous Doppler resonance) the tail relaxes into an isotropic distribution. The role of a convection type loss term is also discussed.

I. INTRODUCTION

Electron acceleration by a dc electric field has been the subject of many analytic and numerical investigations. The presence of high-energy tails has been observed in tokamaks and the Earth's auroral zones. Such tails could also be responsible for many radio bursts during solar flares. Earlier studies on the dynamics of dc electric field acceleration[1–8] have shown that tails formed by sub-Dreicer dc electric fields are unstable to the anomalous Doppler instability and that they relax toward isotropy in two stages. A positive slope region is formed at the leading edge of the tail by preferential pitch-angle scattering of the more energetic electrons at the anomalous Doppler resonance; this drives bump-on-tail plasma instabilities and relaxes quasilinearly.

In a recent numerical study, Wiley *et al.*[9] showed that runaway tails, dynamically driven from a Maxwellian distribution, are marginally unstable. However, since their velocity grid was limited to velocities $v \leqslant 10 - 15\, v_e$ (where v_e is the thermal velocity) they made an analytic parameterization of the distribution functions obtained from their simulations for $v_\parallel < 10\, v_e$, and extrapolated the shape of the distribution function to higher velocities. This extrapolation resulted in an erroneous result, because they missed the instabilities that can be triggered either via the Čerenkov or the anomalous Doppler resonance. Muschietti *et al.*[10] showed that at some stage during the dynamic formation of the runaway tail a positive slope appears on the runaway distribution. This in turn excites plasma waves via the Čerenkov resonance, which at a later time stops the acceleration of the runaway particles along the ambient magnetic field ($v_\parallel$). Pitch-angle scattering of the fast particles by the excited plasma waves then leads to an isotropic quasisteady-state distribution. For this reason it was suggested[10] that any consideration of threshold for instability is unreliable. The anomalous Doppler effect triggers the instability only when a particle source prevents depletion of the bulk distribution and the appearance of the Čerenkov instability.

We constructed a quasilinear code similar to the one used by Muschietti *et al.*[10] and reexamined the dynamic formation of runaway tails. We found that in a relatively large $v_\parallel$ domain ($8\, v_e$ to $60\, v_e$) the runaway tail will sometimes trigger the anomalous Doppler or Čerenkov instability even in the absence of any particle source. The process was a sensitive function of the dc electric field (E_0) and the (cyclotron frequency to plasma frequency) ω_{ce}/ω_{pe} ratio. Our computations demonstrated that for a given ω_{ce}/ω_{pe} ratio and potential drop, particles can be accelerated to higher velocities with a weak dc field (i.e., potential distributed over long distance) rather than with a strong dc field. As will be explained later, these results indicate that for systems where particles are lost when the value of $v_\parallel$ is larger than a critical velocity value v_l, there *will be a threshold for instability*. The particular case where $v_l = 60\, v_e$ corresponds to a stability boundary similar to the one discussed by Liu and Mok[5] for a particular range of E_0/E_D, where E_D is the Dreicer field, and ω_{ce}/ω_{pe} ratios. Computations also show that for a particle loss rate of $1/v_\parallel$ (e.g., if the confinement time $\tau = L/v_\parallel$, where L is the scale length of the system) a power law runaway distribution function results.

In Sec. II we present the model equations and the main assumptions of our study, and in Sec. III we discuss our numerical results. The role of particle losses is analyzed in Sec. IV, and our summary and conclusions are presented in Sec. V.

II. QUALITATIVE CONSIDERATIONS AND MODEL EQUATIONS

Consider a homogeneous magnetized plasma, cylindrically symmetric about the ambient magnetic field, with infinite mass ions, in the low density regime $\omega_{ce} > \omega_{pe}$. Here $\omega_{ce} = eB/mc$ is the electron cyclotron frequency, $\omega_{pe} = (4\pi n_0 e^2/m)^{1/2}$ is the plasma frequency, c is the speed of light, and n_0, m, and e are the electron density, mass, and charge, respectively. If a dc field E_0 is applied to the plasma along the magnetic field, electrons with velocities greater than a critical velocity $v_c = (E_D/E_0)^{1/2} V_e$ can overcome the drag force caused by collisions and run away.[11] The runaway electrons can resonantly interact with two different modes of plasma oscillations: the lower-hybrid (LH) mode $\omega_k = \omega_{pe} k_\parallel / k$ and the upper-hybrid (UH) mode $\omega_k = |\omega_{ce}|(1 + \omega_{pe} k_\perp^2 / 2\omega_{ce} k^2)$. In the low density regime, the growth rate of the LH waves is larger than the growth rate of the UH waves by a factor of ω_{ce}/ω_{pe} [e.g., see Akhiezer *et al.*[12]]. For the sake of simplicity, therefore, we will consider only the LH waves in our study. The wave–particle interaction can take place via the Čerenkov resonance

 0031-9171/85/113356-09$01.90

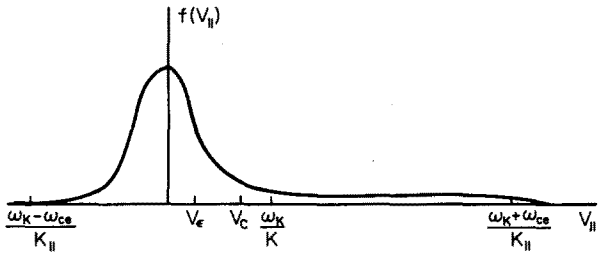

FIG. 1. Positions of the Čerenkov and cyclotron resonances in relation to v_e and v_c.

$\omega_k = k_\parallel v_\parallel$, and the cyclotron resonance $\omega_k + n\omega_{ce} = k_\parallel v_\parallel$, where n is an integer either positive (the anomalous Doppler resonance) or negative (the normal Doppler resonance). For waves propagating in the same direction as the runaway tail ($k_\parallel > 0$), the positions of the Čerenkov and the first harmonics of the cyclotron resonances ($n = 1, -1$) in relation to v_e and v_c are shown in Fig. 1. For a Maxwellian plasma, the number of electrons that will resonate with the waves via the normal Doppler resonance is negligible.[7] Therefore we will ignore the normal Doppler interaction. Also, for $\omega_{ce}/\omega_{pe} > 1$ the contribution from higher harmonics to the growth rates and the diffusion coefficients will be smaller than the contribution from the first harmonic by a factor of n^2. The higher harmonics will also have much higher phase velocities. Therefore, only the $n = 1$ harmonic will be kept in the equations, restricting our study to the anomalous Doppler resonance at velocities $v_\parallel = (\omega_k + \omega_{ce})/k_\parallel \approx \omega_{ce}/k_\parallel$.

We normalize our parameters as follows: $\tilde{v} = v/v_e$, $\tilde{k} = k\lambda_D$, $\tilde{t} = t\omega_{pe}$, $\tilde{f} = f/(n_0/v_e^3)$, $\tilde{W} = W/4\pi n_0 T\lambda_D^3$, and $\tilde{\omega}_{ce} = \omega_{ce}/\omega_{pe}$. Here λ_D is the Debye length, T is the ambient plasma temperature, and W the wave energy density. For the sake of convenience we omit, below, the bar from the dimensionless quantities. The quasilinear diffusion equation, including a model collision term,[13] is given by

$$\frac{\partial f}{\partial t} = \frac{\partial}{\partial v_\parallel} D_0 \frac{\partial f}{\partial v_\parallel} + \left(\frac{\partial}{\partial v_\parallel} - \frac{v_\parallel}{v_\perp}\frac{\partial}{\partial v_\perp}\right) D_1 \left(\frac{\partial f}{\partial v_\parallel} - \frac{v_\parallel}{v_\perp}\frac{\partial f}{\partial v_\perp}\right) - E_0 \frac{\partial f}{\partial v_\parallel} + \frac{\partial}{\partial v_\parallel} \nu(v_\parallel)\left(v_\parallel f + \frac{\partial f}{\partial v_\parallel}\right), \tag{1}$$

where $\nu(v_\parallel) = \nu_0(1 + v_\parallel^2)^{-3/2}$ is the collision frequency, $f \equiv f(v_\parallel, v_\perp, t)$, and

$$D_0(v_\parallel, t) = 2\pi \int_{k_\parallel > 0} \frac{d^3k}{(2\pi)^3}\left(\frac{k_\parallel}{k}\right)^2 \times W_k(t)\delta\left(\frac{k_\parallel}{k} - k_\parallel v_\parallel\right), \tag{2}$$

$$D_1(v_\parallel, t) = \frac{\pi}{2}\int_{k_\parallel > 0} \frac{d^3k}{(2\pi)^3}\left(\frac{k_\parallel}{k}\right)^2 \times W_k(t)\left(\frac{k_\perp v_\perp}{\omega_{ce}}\right)^2 \delta(\omega_{ce} - k_\parallel v_\parallel). \tag{3}$$

The spectral density $|E_k|^2$ will evolve through the equation

$$\frac{\partial W_k(t)}{\partial t} = 2\left(\gamma_0 + \gamma_1 - \frac{\nu_0}{2}\right) W_k(t), \tag{4}$$

where the growth rates caused by the Čerenkov and the anomalous Doppler interactions are given by

$$\gamma_0 = \frac{\pi}{2}\frac{k_\parallel}{k^3}\int d^3v\, k_\parallel \frac{\partial f}{\partial v_\parallel}\,\delta\left(\frac{k_\parallel}{k} - k_\parallel v_\parallel\right) \tag{5}$$

and

$$\gamma_1 = \frac{\pi}{8}\frac{k_\parallel}{k^3}\int d^3v\, k_\parallel \left(\frac{\partial f}{\partial v_\parallel} - \frac{v_\parallel}{v_\perp}\frac{\partial f}{\partial v_\perp}\right) \times \left(\frac{k_\perp v_\perp}{\omega_{ce}}\right)^2 \delta(\omega_{ce} - k_\parallel v_\parallel). \tag{6}$$

Notice that in our units the dc field is normalized to $(4\pi nT)^{1/2}$; therefore the quantity $2E_0/\nu_0$ is the dc field normalized to the Dreicer field and $(\nu_0/E_0)^{1/2}$ is the critical velocity v_c.

Two important observations can simplify the construction of the quasilinear code and the illustration of the wave–particle interaction regions shown in figures for $f(v_\parallel)$ and W_k. First, the Dirac functions involved in the diffusion coefficients and growth rates do not depend on $v_\perp$. Therefore, the distribution function in the perpendicular direction may be treated globally. We will use a moment approach in the perpendicular direction assuming, *a priori*, a Maxwellian shape for the electron distribution in that direction. Therefore,

$$f(v_\parallel, v_\perp, t) \equiv f(v_\parallel, t)\frac{1}{2\pi T_\perp(t)}\exp\left(-\frac{v_\perp^2}{2T_\perp(t)}\right).$$

Second, the growth of the waves depends on the net growth rate $\gamma_0 + \gamma_1$. It is thus difficult to recognize which instability, Čerenkov or anomalous Doppler, drives the unstable modes. To overcome this difficulty, at least during some stages of the runaway tail evolution, one can be guided from the linear analysis. Namely, knowledge of the most unstable modes for each instability (the modes with $k_\perp \approx 0$ for the Čerenkov and the modes with $k_\perp/k_\parallel = \sqrt{2}$ for the anomalous Doppler) and a three-dimensional picture of the wave spectrum may be helpful in this matter. Another useful tool is the projection of the wave spectrum onto $v_\parallel$ space, which can show clearly the regions in $v_\parallel$ space where the wave–particle interaction takes place either via the Čerenkov or the anomalous Doppler, or both. We will use two separate projection operators, $\delta(v_\parallel - k^{-1})$ and $\delta(v_\parallel - \omega_{ce}/k_\parallel)$, to project $W_k(k_\parallel, k_\perp, t)$ onto $v_\parallel$ space. The two spectra represented by I_c and I_D are

$$I_c(v_\parallel, t) = \int_{k_\parallel > 0} \frac{d^3k}{(2\pi)^3} W_k(k_\parallel, k_\perp, t)\delta(v_\parallel - k^{-1}) \tag{7}$$

and

$$I_D(v_\parallel, t) = \int_{k_\parallel > 0} \frac{d^3k}{(2\pi)^3} W_k(k_\parallel, k_\perp, t)\delta\left(v_\parallel - \frac{\omega_{ce}}{k_\parallel}\right). \tag{8}$$

One can clearly see that the total fluctuation energy is

$$W(t) = 2\int_{k_\parallel > 0} \frac{d^3k}{(2\pi)^3} W_k(k_\parallel, k_\perp, t)$$
$$= 2\int_0^\infty I_c(v_\parallel, t)\, dv_\parallel = 2\int_0^\infty I_D(v_\parallel, t)\, dv_\parallel .$$

III. NUMERICAL MODEL AND RESULTS

A quasilinear code based on the Ritz–Galerkin method and special finite elements[10,14–16] was constructed. As mentioned, the distribution function in the direction perpendicular to the magnetic field was taken as Maxwellian and therefore a moment approach was used in that direction. In the parallel direction a kinetic description was kept, and in the semifinite velocity domain $[-8 \lesssim (v_\parallel / v_e) \lesssim 60,\ 0 < v_\perp < \infty]$ the form of the distribution function was assumed to be

$$f(v_\parallel, v_\perp, t) = \sum_{i=1}^{N} f_i(t)\psi_i(v_\parallel) \times \frac{1}{2\pi T_i(t)} \exp\left(-\frac{1}{2}\frac{v_\perp^2}{T_i(t)}\right).$$

Here $\psi_i(v_\parallel)$ is the basis function (roof function),[16] $f_i(t)$ and $T_i(t)$ are the values of $f(v_\parallel)$ and $T_\perp$ at ith grid point, respectively, and N is the number of divisions in equally divided $v_\parallel$ space. Equations (1)–(6) were discretized according to the scheme prescribed in Ref. 14. Depending on the value of the dc field (and accordingly the critical velocity v_c), N was chosen so there were enough points to represent a relatively smooth Maxwellian distribution. In order to discretize the wave spectrum, the finite k space was divided into small rectangles with different sizes.

The rate equations for the field energy were solved in k space. To provide a uniform distribution of modes in terms of their resonant phase velocity, it was necessary to use a nonuniform distribution of modes in k space. This is, of course, simply because of the fact that v_ϕ is inversely proportional to k. In our case, the spacing of the k modes is complicated by the fact that we need to provide sufficient coverage for two different resonances—the Čerenkov and the anomalous Doppler. The parallel velocity domain was divided into N cells of width Δv stretching from $-8\, v_e$ to $v_{\max}$. Since below v_c the waves are heavily damped by the thermal background, the modes with $v_\phi < v_c$ were excluded. To accurately treat the Čerenkov resonance ($v_\phi = k_\parallel^{-1}$), $k_\parallel$ was spaced so that there was a resonant $k_\parallel$ in each Δv between v_c and $v_{\max}$. For the anomalous Doppler resonance ($v_\phi = \omega_{ce} k_\parallel^{-1}$), the interaction region stretched from $\omega_{ce} v_c$ to $v_{\max}$. The density of $k_\parallel$ modes in this region was increased by ω_{ce} over that required for the Čerenkov resonance. This again ensured that there is a resonant $k_\parallel$ for each Δv, and defined the spacing of the modes in $k_\parallel$. For each $k_\parallel$ there were modes covering the $k_\perp$ direction from $k_\perp \approx 0$ to $k_\perp \approx 0.15$. The typical k-space grid used was (100, 20). The discretized wave spectrum was assumed to have a form

$$W_k(k_\parallel, k_\perp, t) = \sum_{l=1}^{L}\sum_{m=1}^{M} \phi_{lm}(k_\parallel, k_\perp) W_{lm}(t),$$

where $\phi_{lm}(k_\parallel, k_\perp)$ is a piecewise constant basis function

$$\phi_{lm}(k_\parallel, k_\perp) = \begin{cases} 1, & \text{in the rectangle numbered } lm, \\ 0, & \text{elsewhere.} \end{cases}$$

A leap-frog scheme was used to advance $f_i(t)$, $T_i(t)$, and $W_{lm}(t)$ in time similar to the scheme prescribed in Ref. 15. Considering four consecutive times t_1, t_2, t_3, and t_4 and knowing $f(v_\parallel, t_1)$, $T_\perp(v_\parallel, t_1)$, and $W_k(k_\parallel, k_\perp, t_2)$, we find f and $T_\perp$ at t_3, and W_k at t_4.

Since different time scales are involved in the dynamic evolution of the runaway tails,[10] we let the time steps $\Delta t_1 = t_3 - t_1$ and $\Delta t_2 = t_4 - t_2$ adjust themselves automatically to fit the dictated time scale. Assuming $\Delta t_1' = t_2 - t_1$, $\Delta t_2' = t_3 - t_2$, and $\Delta t_3' = t_4 - t_3$, and considering $\Delta t_2' = \alpha \Delta t_1'$ and $\Delta t_3' = \alpha \Delta t_2'$, where $\alpha = [(10 \pm 1)/10]^{1/2}$, we achieve fast time step adjustment without destroying the centering of the times t_2 and t_3. Starting with a Maxwellian distribution for $f(v_\parallel, v_\perp, t = 0)$ and thermal noise for $W_k(t = 0)$, we made several runs with dc fields of different strengths (0.08 to 0.45 E_D) and $\omega_{ce}/\omega_{pe} = (2$ to $5)$. For strong dc fields ($E_0/E_D \gtrsim 0.12$), the evolution of the wave–particle system was qualitatively similar to the one reported by Muschietti *et al.*[10] However, for dc fields $E_0/E_D \lesssim 0.1$, the instability of the system (in the chosen velocity limits) depends on ω_{ce}/ω_{pe}. In fact, as we will discuss in Sec. III B, the instability was triggered at the anomalous Doppler resonance.

In the following we first analyze the evolution of the distribution function and wave spectrum for the electric field values $E_0 = 0.2\, E_D$ and $E_0 = 0.1\, E_D$. We then discuss the threshold for the instability and present results showing the dependence of the current, the runaway rate, and the number density of the runaway particles on the value of E_0.

A. Strong dc field ($E_0/E_D = 0.2$)

In this run, the system was initialized with a Maxwellian distribution for the electrons and white noise for the wave spectrum [$W_{lm}(k_\parallel, k_\perp, t = 0) = T$, where T is the temperature of the bulk]. The time step adjusts itself automatically to the runaway growth time, with an upper bound of $(1/200)\,\tau_s$ (where $\tau_s = \nu_0^{-1}$ is the collision time). During the first 170 τ_s, a long runaway tail with a small negative slope on the plateau portion of the tail develops. As the tail reaches higher $v_\parallel$ values, a small positive slope appears on the runaway tail. Formation of this positive slope is caused by the bulk depletion and the decrease of the drag force on the particles as they are accelerated. The positive slope excites Langmuir waves and relaxes quasilinearly, leaving behind a flat tail distribution $[(\partial f/\partial v_\parallel)|_{v_\parallel \approx 14 v_e} \approx 0]$ and a spectrum of waves that are centered at phase velocity $v_\phi \approx 14$ [Fig. 2(a)]. As can be seen at the time of the appearance of the wave spectrum, the lower edge of the I_D spectrum is far away from the leading edge of the tail. This indicates that the waves are excited via the Čerenkov effect and there is as yet no interaction between the excited waves and particles via the anomalous Doppler effect.

As the tail stretches in $v_\parallel$ space, $T_\perp$ remains almost equal to 1 and the wave spectrum is sustained (and broadened in the course of time) on the runaway tail, until the leading edge

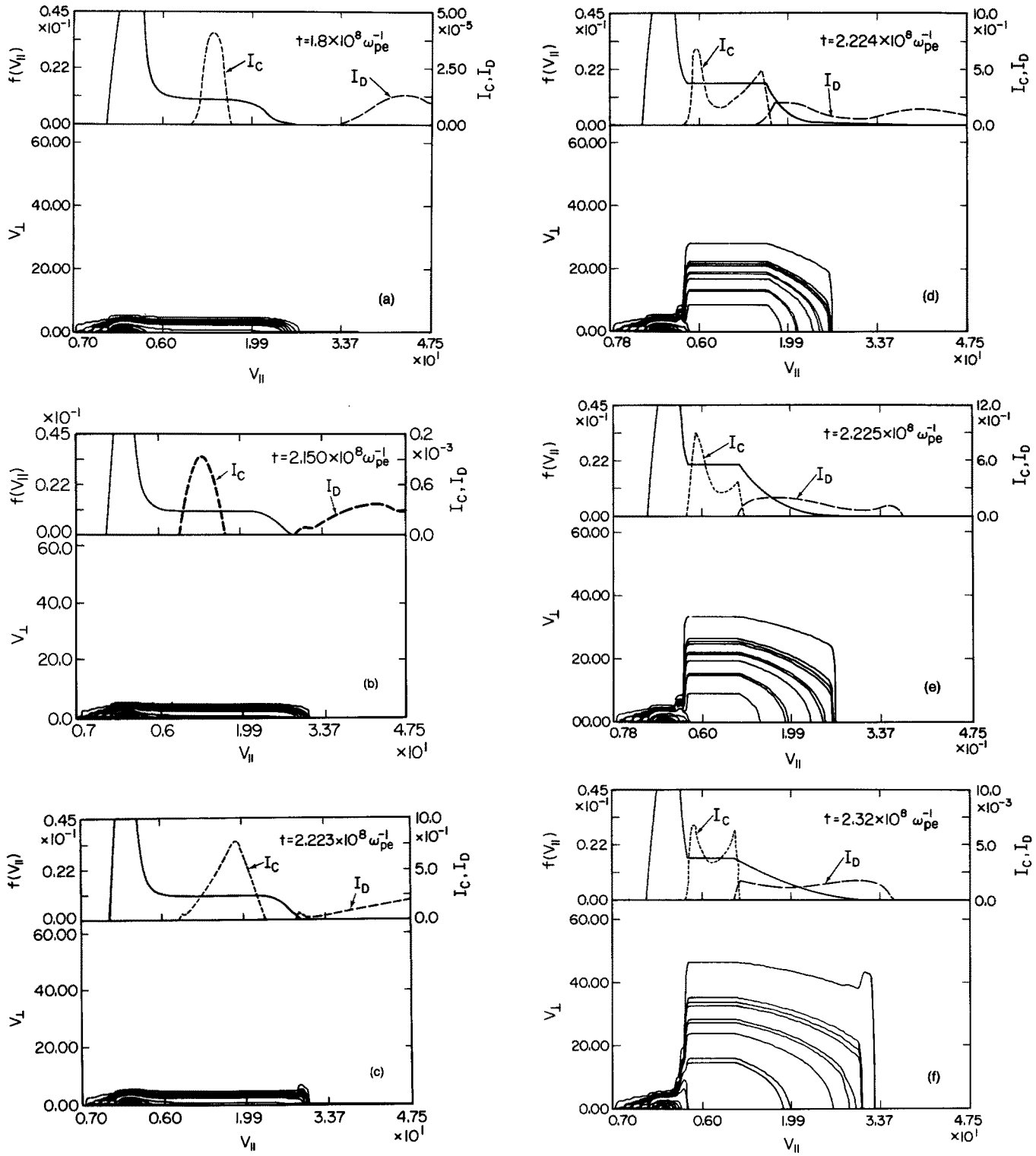

FIG. 2. Electron distribution function and wave spectrum at six different times. I_c and I_D are projections of the wave spectrum onto $v_\parallel$ space via Eqs. (7) and (8). (a) Onset of turbulence. (b) The runaway tail reaches the I_D spectrum. (c) Few collision times after the tail stops growing. (d) Relaxation period of the distribution function toward isotropy. (e) Final stage of the tail retraction. (f) Quasisteady state. Parameters used are $E_0/E_D = 0.2$, $\omega_{ce}/\omega_{pe} = 3$, $\nu_0/\omega_{pe} \approx 10^{-6}$.

of the tail reaches the lower edge of the I_D spectrum [Fig. 2(b)]. At this time, strong pitch-angle scattering occurs for the fast particles that satisfy the Doppler resonance condition. The tail stops expanding in $v_\parallel$. In a very short time (a few collision times), the waves with phase velocities below the lower edge of the I_c spectrum, being excited via the anomalous Doppler interaction, are Landau damped to set up a real plateau in that portion of the tail [Fig. 2(c)]. After the formation of a plateau below the lower edge of the I_c spectrum, which can support the waves excited via the

anomalous Doppler effect, for a very short time [about $(1/20)\,\tau_s$] an interplay between anomalous Doppler effect and Čerenkov effect isotropizes the distribution function.[10]

In the isotropization process, the pitch-angle scattering of the fast particles by the waves, which is a nearly elastic process,[17] increases the perpendicular kinetic energy of the fast particles at the expense of their parallel kinetic energy. Therefore this process diffuses fast particles backward in $v_\parallel$ space, resulting in the formation of a small bump at the outer end of the plateau.[7] The flattening of this small bump by the Čerenkov effect results in the redistribution of the electrons with high gyration energy and excitation of the waves all along the plateau. In this manner the tail shrinks slowly while $T_\perp$ increases along the tail. Since during the isotropization process the system is unstable to both the Čerenkov and the anomalous Doppler instabilities, the waves are excited via both effects ($\gamma_0 > 0$, $\gamma_1 > 0$). A typical distribution function and wave spectrum during the isotropization process is shown in Fig. 2(d). At the end of this stage the distribution function is characterized by a short tail beyond v_c in the parallel direction with a large temperature in the perpendicular direction [Fig. 2(e)]. The runaway tail has a very small positive slope $[\partial f(v_\parallel)/\partial v_\parallel \approx 10^{-6}]$ between v_c and $v_D = \omega_{ce} v_c$ and it is isotropic beyond v_D:

$$F(v_\parallel) = F(v_D)\exp[-(v_\parallel^2 - v_D^2)/2T_\perp], \quad v_\parallel > v_D. \quad (9)$$

After the establishment of the plateau boundaries at v_c and v_D the excited waves with phase velocities $v_c < v_{ph} < v_D$ are damped by the collisions in a few collision times. The wave level decreases by a few orders of magnitude but it does not drop to the noise level [Fig. 2(f)]. The system reaches a quasisteady state during which, while the distribution function remains isotropic, the energy provided by the E_0 field goes to the waves and in turn via collisions the energy returns to the thermal reservoir. Using. Eq. (9) we calculated $f(v_\parallel)$ for $v_\parallel > v_D$. The numerical values and the values from Eq. (9) are shown in Fig. 3 at two different times: at the time of the establishment of plateau boundaries, and after the damping of the excited waves by collisions (quasisteady state). The close fitting of Eq. (9) and our numerical results indicates

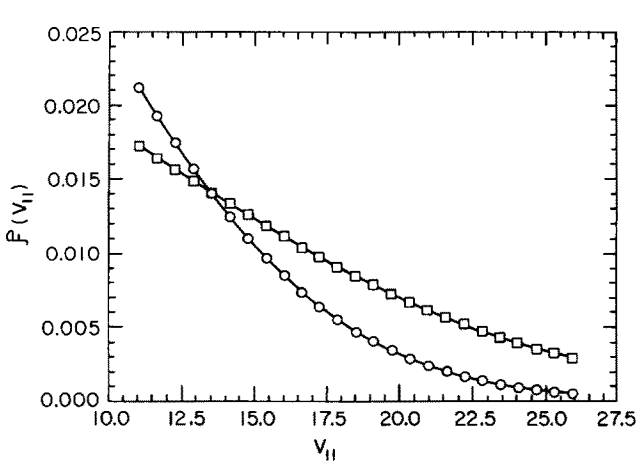

FIG. 3. Electron distribution function beyond $v_\parallel = (\omega_{ce}/\omega_{pe})v_c$. Square marks and circle marks are from Fig. 2(e) and Fig. 2(f), respectively. The solid lines are the values obtained using Eq. (9).

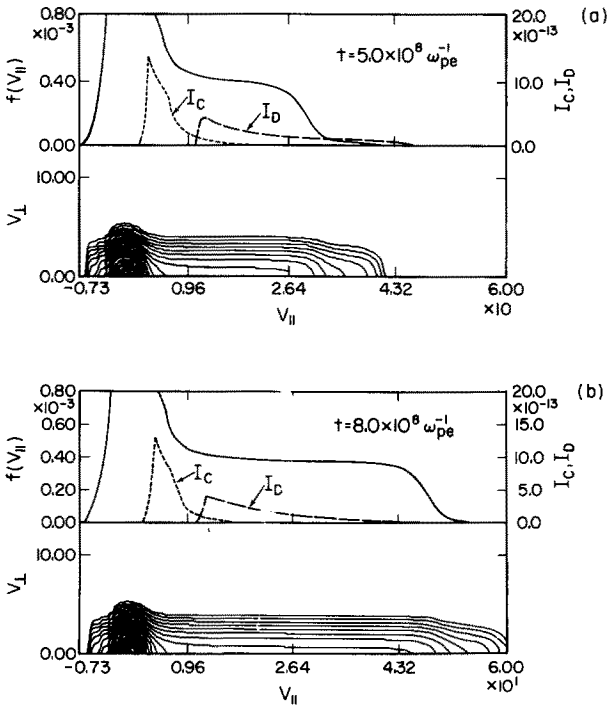

FIG. 4. Electron distribution function and wave spectrum (noise level) at two different times. Here, I_c and I_D are projections of the noise (white noise) onto $v_\parallel$ space via Eqs. (7) and (8). (a) A typical state during tail growth. (b) Final state of the system. The leading edge of the tail has reached $v_\parallel = 60\,v_e$. The parameters used are: $E_0/E_D = 0.1$, $\omega_{ce}/\omega_{pe} = 3$, $\nu_0/\omega_{pe} \approx 10^{-6}$.

that we have reached the quasisteady state and the formation of the isotropic distribution discussed above.

B. Weak dc field ($E_0/E_D = 0.1$)

1. $\omega_{ce}/\omega_{pe} = 3$

Starting again with a Maxwellian distribution and noise spectrum, a runaway tail with $T_\perp \approx 1$ grows out of the Maxwellian distribution. It takes about 800 τ_s until the outer edge of the tail reaches to $v_\parallel = 60$. As the tail grows its slope remains negative $[\partial f(v_\parallel)/\partial v_\parallel \approx -1.\times10^{-6}$, at $f(v_\parallel) \approx 4\times10^{-4}]$ and the wave spectrum stays at the noise level [Fig. 4 (a) and (b)]. Although there is a large anisotropy in the distribution function ($T_\parallel > T_\perp$), the runaway distribution is stable because of the presence of the negative slope.

2. $\omega_{ce}/\omega_{pe} = 2$

For this case, a runaway tail, similar to the one in Sec. III B 1 grows out of the Maxwellian distribution. The wave spectrum stays near noise until the leading edge of the tail reaches the velocity $v_\parallel \approx 50\,v_e$. At this moment one of the oblique modes $[k_\perp/k_\parallel \approx \tan(54°)]$ starts growing. This stage is shown in Fig. 5. At the time that the instability starts growing there is a negative slope on the velocity distribution $f(v_\parallel)$ at $v_\parallel = v_\phi$ (v_ϕ is the phase velocity of the growing mode). However, there are enough particles near the outer end of the plateau to sustain $\gamma_1 + \gamma_0 - \nu_0/2 > 0$. The growth of the mode with $(k_\perp^2/k_\parallel^2) = [\tan(54°)]^2 \approx 2$ indicates the instability of the most unstable waves to the anomalous Doppler effect. Therefore, the turbulence is triggered via the

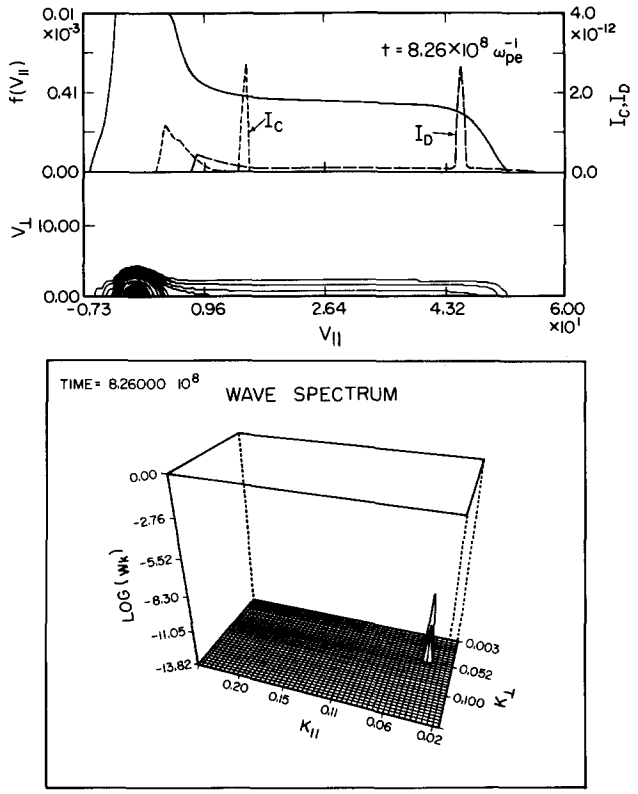

FIG. 5. Typical electron distribution and wave spectrum at the time of the start of instability via the anomalous Doppler effect. Here, I_c and I_D are projection of the wave spectrum (noise plus initial growing mode) onto $v_\parallel$ via Eqs. (7) and (8). The initial growing mode is at an angle of 54° with respect to the $k_\parallel$ axis. The parameters used are: $E_0/E_D = 0.1$, $\omega_{ce}/\omega_{pe} = 2$, $\nu_0/\omega_{pe} \approx 10^{-6}$.

anomalous Doppler resonance considered in the analytical studies discussed in the introduction. The only difference between some of the analytical treatments[4,5] and our numerical result is that here the waves with $v_\phi \approx 15\, v_e$, which is about $3v_c$, start growing (unlike the analytical studies where it is assumed that the unstable waves will have $v_\phi \approx v_c$).

After the start of the instability, the particle distribution evolves toward isotropy in a fashion similar to the one discussed for the strong dc electric fields above.

C. Threshold for instability, runaway rate, maximum velocity, and current

1. Threshold for instability

In many real systems, particles that reach very high velocities can be lost from the system (e.g., because of imperfect magnetic surfaces). To model this, we considered a limited $v_\parallel$ in our numerical computations ($v_{\parallel\,\max} = 60\, v_e$). The following discussion on the instability threshold is based on this consideration.

Several runs with dc field values ranging from $0.45\, E_D$ to $0.07\, E_D$, ω_{ce}/ω_{pe} ratios of 2 to 5, and $\nu_0 = 10^{-6}$ were performed. We found four different regimes in the evolution of the runaway tail (shown in Fig. 6).

Regime I: The evolution of the wave particle system was discussed in Sec. IIIA and by Muschietti *et al.*[10] A positive slope caused by the depletion of the bulk is formed at the

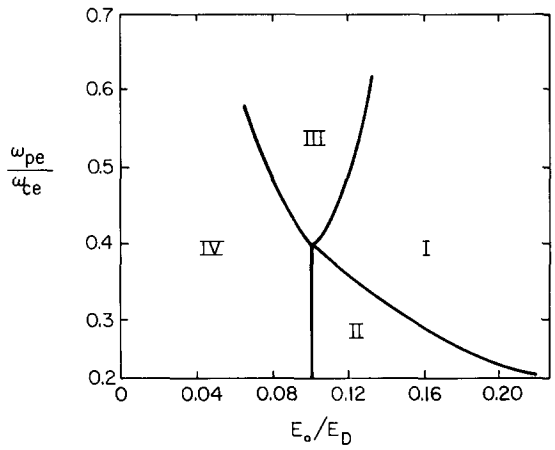

FIG. 6. Stability boundaries when the maximum $v_\parallel$ boundary is $60\, v_e$. In regions I and II, instability is triggered via the Cerenkov effect. However, for the tails that are formed in region II, pitch-angle scattering of the fast particles cannot be triggered. In region III the instability is triggered via the anomalous Doppler effect. In region IV the system is marginally stable.

beginning, plasma waves are excited, and the anomalous Doppler shifted waves pitch-angle scatter the edge of the tail. The final stage is an isotropic distribution.

Regime II: The positive slope develops for large velocities and the anomalous Doppler shifted spectrum is outside the $v_{\parallel\,\max} \simeq 60\, v_e$. The particles do not reach the anomalous Doppler shifted waves and the pitch-angle scattering is not triggered.

Regime III: The tail stretches to high velocities ($\simeq 50\, v_e$) and maintains a negative slope, but the anomalous Doppler instability is triggered by the large velocity anisotropy in the tail. The tail subsequently relaxes to an isotropic distribution, in a fashion similar to the one discussed in Sec. III A.

Regime IV: The runaway tail maintains a negative slope and the wave spectrum remains at the noise level until the leading edge of the tail reaches the $v_{\parallel\,\max}$ velocity.

2. Runaway rate

Using the numerical values for $f(v_\parallel, t)$, the number of runaway electrons and the runaway rate are computed using the equations

$$\frac{\Delta n(t)}{n_0} = \int_{v_c}^{\infty} f(v_\parallel, t)\, dv_\parallel ,$$

$$\Gamma = \int_{v_c}^{\infty} \frac{\partial f(v_\parallel, t)}{\partial t}\, dv_\parallel \equiv \frac{\partial}{\partial t}\left(\frac{\Delta n(t)}{n_0}\right),$$

where n_0 is the initial density. Figure 7 shows the time evolution of Γ for a range of E_0. At the beginning of the tail formation, Γ reaches a maximum. During this initial stage the evolution of Γ agrees with the simulations made by Wiley *et al.*[9] However, because of bulk depletion, the runaway rate decreases from this moment forward.

In Fig. 8 we show the dependence of the maximum runaway rate ($\Gamma_{\max}$), Γ_{tu} (where tu refers to the value of the runaway rate at the time of the appearance of positive slope on the runaway distribution), and the classical runaway rate,

$$A = \frac{\nu_0}{\sqrt{2\pi}}\left(\frac{E}{\nu_0}\right)^{3/2} \exp\left[-\frac{1}{4}\left(\frac{\nu_0}{E}\right)\right],$$

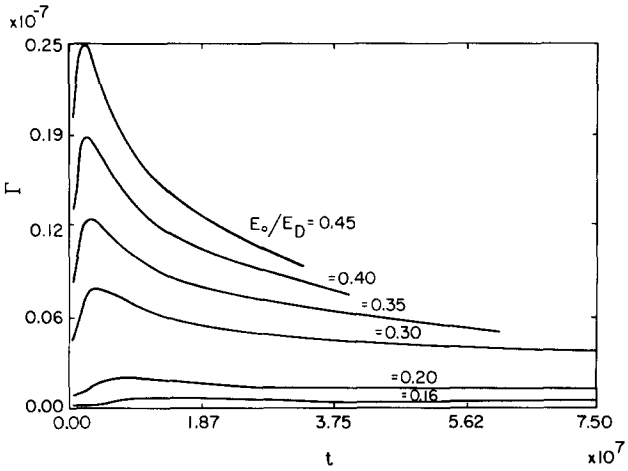

FIG. 7. Evolution of the runaway rate Γ for different dc fields.

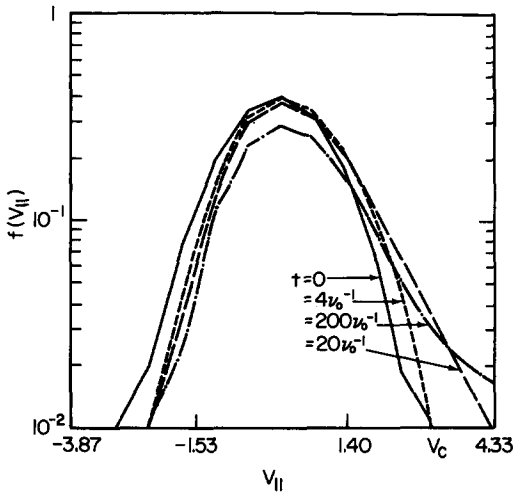

FIG. 9. Deformation of the distribution function near $v_{\parallel} \approx v_c$ at the time of tail formation.

where $2(E_0/\nu_0)$ is the dc field normalized to E_D, on E_0. As can be seen, A is smaller than the corresponding numerical runaway rates Γ_{max} and Γ_{tu}. The reason for this increase in the runaway production rate is that at the start of the tail formation the shape of the distribution function (which is not considered in the analytical calculation of A) near $v_{\parallel} = v_c$ deviates considerably from a Maxwellian distribution in such a way that more particles can overcome the drag force caused by collisions and run away (Fig. 9). Also, part of the increase can be attributed to the Landau damping of Langmuir waves near $v_{\parallel} = v_c$, (which can be excited via the anomalous Doppler interaction) that pull more particles out of the bulk. In Fig. 10 the dependence of $\Delta n/n_0$ vs E_0 is shown. Although the runaway rate increases with the increase in E_0, the maximum velocity that the particles achieve decreases (see below). These two parameters control $\Delta n/n_0$ in such a way that it reaches an asymptotic value (which depends on ω_{ce}/ω_{pe}).

3. Maximum velocity (v_{max})

We have shown that the pitch-angle scattering of the fast particles by the excited waves does not allow the tail to stretch beyond a certain velocity. In Fig. 10 we plot maximum velocity v_{max} as a function of E_0 for $\omega_{ce}/\omega_{pe} = 3$. We found that the maximum velocity increases as the E_0 decreases. In fact, for $E_0 < 0.1$, the tail can practically stretch beyond 60 v_e.

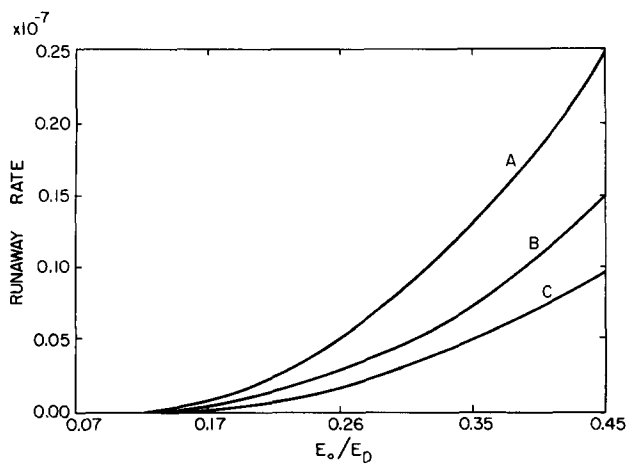

FIG. 8. Runaway rates versus dc field: A—maximum values of the curves in Fig. 6, B—at the onset of turbulence, C—classical.

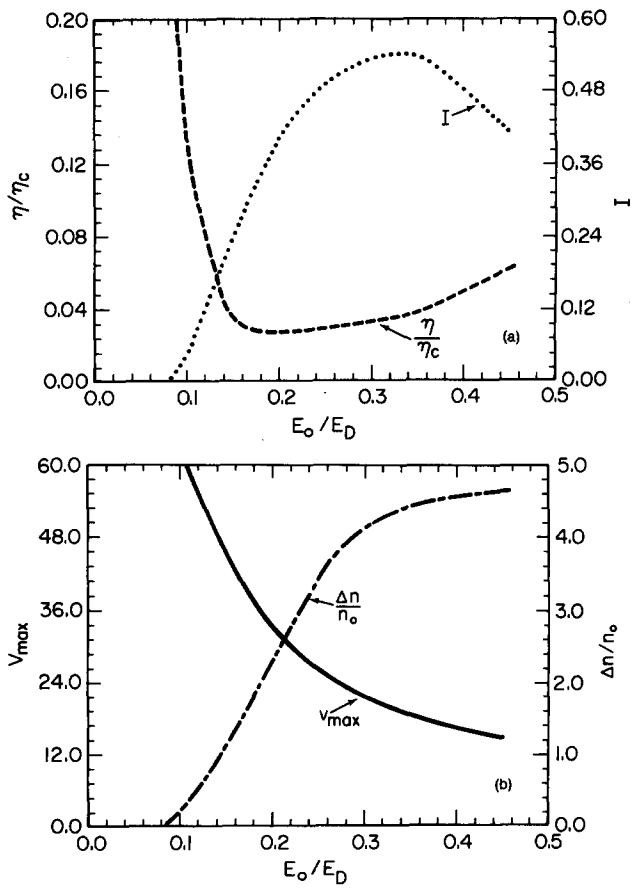

FIG. 10. Dependence on dc field of a) resistivity η (normalized to the classical resistivity η_c) and current I; (b) number of particles in the tail $\Delta n/n_0$ and maximum velocity that the leading edge of the tail can reach before the start of pitch-angle scattering.

4. Current and resistivity

Although the number of runaways prior to the tail retraction increases with the increase of the dc field, the particles can not be accelerated to as high a velocity. In Fig. 10 we show the dependence of the current (at the time that the tail stops growing in $v_{\parallel}$) versus E_0, where the normalized current is computed using the equation

$$J = \int_{v_c}^{\infty} dv_{\parallel}\, v_{\parallel} f(v_{\parallel}).$$

In the range of $0 < E_0 \leqslant 0.25$ the current increases with increase in E_0. In the range 0.25 to 0.35 it has a maximum value, and then drops for $E_0 \gtrsim 0.35$. The behavior of the resistivity $\eta = E_0/J$ vs E_0 is shown in Fig. 10.

IV. PARTICLE LOSS

In the analysis presented above we assumed that particles are lost only when they exceed a maximum velocity ($v_{\parallel \max}$). We now introduce a convective loss term in Eq. (1) by subtracting the term $f(v_{\parallel})/\tau$ from the right-hand side of Eq. (1), where $\tau = L/|v_{\parallel}|$ and L is the scale length of the system. Using a strong dc electric field value, $E_0 = 0.3\, E_D$ and $\omega_{ce}/\omega_{pe} = 3$, we found that, depending on the length L of the system, the runaway tail may evolve in three different ways.

(i) For $L > 5\times 10^9 \lambda_D$, the evolution of the wave–particle system is the same as for $L = \infty$, and the particle loss term does not prevent the appearance of the positive slope on runaway tail during its formation. Therefore, the excitation of plasma waves via the Čerenkov effect during this stage, which pitch-angle scatters fast particles in the leading edge of the tail at a later time, prevents the tail from stretching too far in $v_{\parallel}$ space. The evolution of the system is similar to the one discussed in Sec. IIIA.

(ii) For $L \lesssim 5\times 10^8 \lambda_D$, a large number of energetic particles are lost and a power law tail develops on the distribution function

$$f(v_{\parallel}) \propto v_{\parallel}^{-\beta}, \quad v_{\parallel} > v_c,$$

where β is time dependent. A typical distribution function is shown in Fig. 11(a).

(iii) For $5\times 10^8 \lambda_D < L < 5\times 10^9 \lambda_D$, a situation arises in which, despite the fast bulk depletion, the slope of the runaway tail remains slightly negative. Therefore a large number of particles can be accelerated to very high velocities [Fig. 11(b)].

It is obvious that with smaller dc electric fields ($E_0 \sim 0.1$ to $0.2\, E_D$) where the bulk depletion is not as fast as for $E_0 = 0.3\, E_D$, it is possible to arrive at marginally stable runaway distributions even at very large L sizes. The implication of these results on astrophysical plasmas will be discussed elsewhere.

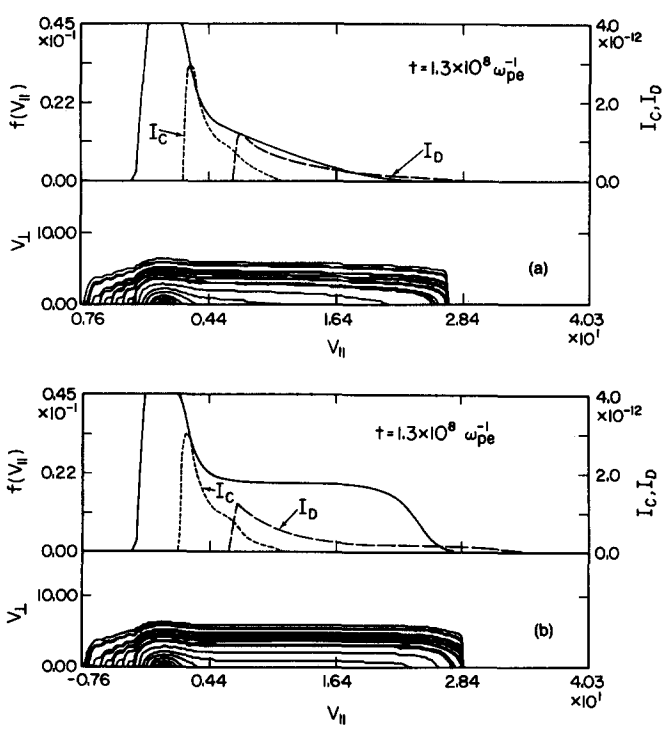

FIG. 11. Typical electron distribution function and wave spectrum (noise) when there is a convection loss term $f(v_{\parallel})|v_{\parallel}|/L$ in Eq. 3: (a) $L = 3\times 10^8 \lambda_D$, (b) $L = 2\times 10^9 \lambda_D$. Other parameters used are $E_0/E_D = 0.3$, $\omega_{ce}/\omega_{pe} = 3$, and $\nu_0/\omega_{pe} \approx 10^{-6}$.

V. SUMMARY AND CONCLUSIONS

We studied the dynamic formation of runaway tails in magnetized plasmas using a nonrelativistic quasilinear numerical code base on the Ritz–Glarkin method. This study was carried out for different sub-Dreicer dc electric fields and with ω_{ce}/ω_{pe} ratios ranging from 2 to 5. Assuming that particles with velocities $v_{\parallel} > 60\, v_e$ will escape from our system, we have reached the following conclusions:

(1) There are four different regimes in the evolution of the runaway tails. In Regime I (shown in Fig. 6) the electric field is strong and the rate with which electrons diffuse from the bulk to high velocities cannot compete with the acceleration rate at the tail. As a result, a positive slope is formed on the tail that excites a spectrum of plasma waves through the Čerenkov resonance. The average phase velocity of the excited plasma waves approaches the bulk of the plasma as the dc electric field approaches the Dreicer field. In this regime the projection of the plasma waves onto $v_{\parallel}$ space by the projector $\delta(\omega_{ce} - k_{\parallel} v_{\parallel})$, which is the anomalous Doppler shift of the excited Langmuir waves, is below $60\, v_e$. As the leading edge of the tail reaches this spectrum, the particles are pitch-angle scattered. This results in an increase in the perpendicular kinetic energy of the fast particles and formation of a small bump at the leading edge of the plateau. Excitation of the plasma waves by the positive slope diffuses the electrons with high gyration energy toward the bulk, which raises the perpendicular temperature along the tail. This interplay between the anomalous Doppler and the Čerenkov resonances continues until the tail distribution is isotropized. For weaker electric fields, the positive slope caused by the bulk depletion is shifted to higher velocities and the anomalous Doppler-shifted spectrum is above $v_{\parallel} = 60\, v_e$. In this case (Regime II in Fig. 6) the tail remains stable. For weak electric fields and $\omega_{ce}/\omega_{pe} < 2$ (Regime III), the runaway tail excites the anomalous Doppler instability first and the isotropization proceeds in a fashion similar to the one discussed for the

Regime I. In Regime IV, where $\omega_{ce}/\omega_{pe} > 2$ and $E_0/E_D \lesssim 0.1$, the tail remains stable until the leading edge of the tail reaches $v_\parallel = 60\, v_e$. This indicates that for a given ω_{ce}/ω_{pe} the runaway electrons can achieve higher velocities by weak dc fields than by the strong dc fields.

(2) For a given ω_{ce}/ω_{pe} ratio and a conserved number of particles, we found that the average runaway rate is larger than the value estimated by the classical runaway rate. We offer two explanations for this discrepancy: (a) The distribution function deviates from the Maxwellian distribution function near the critical velocity at the start of the tail formation. This change on the velocity distribution allows more particles to run away. (b) Another cause for the higher runaway rate is the Landau damping of the waves near v_c that were excited by the anomalous Doppler resonance.

(3) The runaway current density (at the time that pitch-angle scattering of the fast particles starts) has a maximum value at $E_0 \simeq 0.3\, E_D$.

(4) We showed that a particle loss term modeled as $f(v_\parallel)v_\parallel/L$, where L is the size of the system, will greatly affect the system evolution if $L \leqslant 5\times 10^9\, \lambda_D$ (for $E_0 = 0.3\, E_D$). For $L < 5\times 10^8\, \lambda_D$ and $E_0 \leqslant 0.3\, E_D$, a power law tail is formed and a large number of electrons are accelerated to high velocities.

The model used in this study treated the detailed shape of the electron distribution in $v_\parallel$, but the transverse velocity distribution was represented by a $T_\perp$. Rowland *et al.*[18] presented the first simulations of the effects of the anomalous Doppler instability on a runaway tail that was formed and driven by a parallel dc field. These simulations employed a self-consistent electrostatic particle code that followed all three velocity components. Both the parallel and perpendicular velocity distribution were represented by simulation particles. This paper presented a model based on strong turbulence anomalous resistivity to explain the acceleration of auroral electrons by parallel dc fields. While *the dc field used in these particle simulations was much larger than* E_D, the scattering and perpendicular heating of the runaway electrons was qualitatively the same as in the simulations reported here. One of the key observational characteristics of this process is that the electrons are first accelerated parallel to the magnetic field forming a strongly field aligned beam. When they are accelerated above a critical velocity (or energy), pitch-angle scattering will act to isotropize the beam. Lin and Rowland[19] recently reported the observation of such two-step acceleration of auroral electrons by the Atmospheric Explorer-D satellite.

Our work is based on nonrelativistic quasilinear equations; thus we restricted our calculation on velocity ($v_\parallel \leqslant 60\, v_e$). Depending on the thermal temperature of the bulk, our upper velocity boundary can be relativistic (e.g., in tokamaks, the thermal temperature is so high that even electrons with velocity $\simeq$20–60 v_e will be relativistic). It is obvious that relativisitic effects will play a significant role in the tail dynamics since, as electron velocity approaches the speed of light, the particles will pile up. This may destabilize the runaway tail even for weak dc fields. This work is clearly beyond the scope of our present study. We have also excluded the effect that a finite plasma will have on the excited waves. It has been shown analytically[20,21] that oblique modes can convect out of the system and modify the behavior of the runaway evolution.

ACKNOWLEDGMENTS

The present research is part of the Ph.D. thesis of one of the authors (E.M.T.).

This work was supported by the National Aeronautics and Space Administration under grant No. NAGW 81. Computational work has been supported in part by the Computer Science Center of the University of Maryland. This work was also supported by Contract Nos.ONR N00014-79-C-0665 and NSFATM 8500794.

[1] V. V. Parail and P. O. Pogutse, Fiz. Plazmy **2**, 228 (1976) [Sov. J. Plasma Phys. **2**, 126 (1976)].
[2] V. V. Parail and P. O. Pogutse, Nucl. Fusion **18**, 303 (1978).
[3] K. Papadopoulos, B. Hui, and N. Winsor, Nucl. Fusion **17**, 1087 (1977).
[4] C. Liu, Y. C. Mok, K. Papadopoulos, F. Engelmann, and M. Bornatici, Phys. Rev. Lett. **39**, 701 (1977).
[5] C. S. Liu, and Y. C. Mok, Phys. Rev. Lett. **38**, 162 (1977).
[6] B. H. Hui and N. Winsor, Phys. Fluids **21**, 940 (1978).
[7] I. Haber, J. D. Huba, P. Palmadesso, and K. Papadopoulos, Phys. Fluids **21**, 1013 (1978).
[8] D.-I. Choi and W. Horton, Plasma Phys. **20**, 903 (1978).
[9] J. C. Wiley, D.-I. Choi, and W. Horton, Phys. Fluids **23**, 2193 (1980).
[10] L. Muschietti, K. Appert, and J. Vaclavik, Phys. Fluids **25**, 1187 (1982).
[11] H. Dreicer, Phys. Rev. **115**, 238 (1959).
[12] A. I. Akheizer, I. A. Akhiezer, R. V. Polovin, A. G. Stienko, and K. N. Stepanov, in *Plasma Electrodynamics* (Pergamon, New York, 1975), Vol. 2, p. 69.
[13] A. A. Vedenov, *Theory of Turbulent Plasma* (London Iliffe, London, 1968).
[14] L. Muschietti, K. Appert, and J. Vaclavik, Phys. Fluids **24**, 151 (1981).
[15] K. Appert, T. M. Tran, and J. Vaclavik, Comput. Phys. Commun. **12**, 135 (1976).
[16] G. Strang and G. J. Fix, *An Analysis of the Finite Element Method* (Prentice-Hall, Englewood Cliffs, NJ, 1973).
[17] B. B. Kadomtsev and P. O. Pogutse, Zh. Eksp. Teor, Fiz. **53**, 2025 (1967) [Sov. Phys. JETP **26**, 1146 (1968)].
[18] H. L. Rowland, P. J. Palmadesso, and K. Papadopoulos, Geophys. Res. Lett. **8**, 1257 (1981).
[19] C. S. Lin and H. L. Rowland, J. Geophys. Res. **90**, 422 (1985).
[20] K. Molvig, M. S. Tekula, and A. Bers (private communication).
[21] K. Molvig, M. S. Tekula, and A. Bers, Phys. Rev. Lett. **38**, 1404 (1977).